Published in final edited form as:
Nat Photonics. 2009 August 29; 3(9): 503–509. doi:10.1038/nphoton.2009.157.

Multiscale photoacoustic microscopy and computed tomography

Lihong V. Wang
Optical Imaging Laboratory, Department of Biomedical Engineering, Washington University in St. Louis, Campus Box 1097, One Brookings Drive, St. Louis, MO 63130-4899

Lihong V. Wang: LHWang@biomed.wustl.edu

Abstract

Photoacoustic tomography (PAT) is probably the fastest growing biomedical imaging technology owing to its capability of high-resolution sensing of rich optical contrast *in vivo* at depths beyond the optical transport mean free path (~1 mm in the skin). Existing high-resolution optical imaging technologies, such as confocal microscopy and two-photon microscopy, have fundamentally impacted biomedicine but cannot reach such depths. Taking advantage of low ultrasonic scattering, PAT indirectly improves tissue transparency by 100 to 1000 fold and consequently enables deeply penetrating functional and molecular imaging at high spatial resolution. Further, PAT holds the promise of *in vivo* imaging at multiple length scales ranging from subcellular organelles to organs with the same contrast origin, an important application in multiscale systems biology research.

1. Introduction

Definition of photoacoustic tomography: old physics and new technology

Photoacoustic tomography (PAT),[1–3] also referred to as optoacoustic tomography, is defined as cross-sectional or three-dimensional (3D) imaging of a material based on the photoacoustic effect. Planar imaging without depth resolution or one-dimensional (1D) depth-resolved imaging does not belong to tomography. In the photoacoustic phenomenon, light is absorbed by a material and converted to heat, and subsequently an acoustic wave is generated due to thermoelastic expansion. PAT—a hybrid of optical imaging and ultrasound imaging—combines rich optical contrast and high ultrasonic resolution in a single modality. PAT is capable of providing high-resolution structural, functional,[4–7] and molecular[8–13] imaging *in vivo* in optically scattering biological tissue at unprecedented depths. While structural imaging cannot differentiate live and dead tissues, functional imaging can do so by measuring physiological functions, such as the blood flow and oxygenation. In addition, molecular imaging can sense biomarkers to identify specific cancer cells or detect gene expression products to track gene activations.

The milestones of PAT and its precursor are briefly summarized here. One hundred years after Bell reported the photoacoustic effect in 1880,[14] Bowen envisioned its potential for imaging with the excitation of ionizing radiation (high-energy electrons, x-ray photons, neutrons, and other charged particles) or non-ionizing radiation (radiowaves, microwaves, and ultrasonic waves).[15] He illustrated 1D depth-resolved imaging using radiowave excitation but never mentioned the possibility of using optical excitation. Ten years later, laser-induced photoacoustic depth-resolved imaging was achieved initially with no or poor (e.g., ~6 mm)

L. W. is the author to whom correspondence and requests for materials should be addressed.

9. Competing interests statement
The author has a financial interest in Microphotoacoustics, Inc. and Endra, Inc., which however did not support this work.

lateral resolution in the direction perpendicular to the acoustic axis.16–20 To acquire cross-sectional or 3D images that are both axially and laterally resolved, PAT based on an approximate reconstruction algorithm was developed;21 alternatively, PAT based on tightly focused ultrasonic detection was attained.22 In 2003, *in vivo* functional PAT was reported.[4] The subsequent rapid growth of research on PAT is highlighted in this article.

Rationale for optical imaging: rich optical contrast

Although many biomedical imaging modalities exist, their limitations call for new imaging technologies. Optical imaging is a strong contender primarily because of its rich contrast. From the safety perspective, light is nonionizing radiation with photon energy of the order of 2 electron volts, whereas x-ray has photon energy of thousands of electron volts and can consequently cause carcinogenesis. From the physics perspective, optical signals are related to the molecular constituents of tissue and hence can provide biochemical information. From the optics perspective, optical absorption is related to various intrinsic contrast origins, such as oxygenated and deoxygenated hemoglobin, melanin, lipids, and even water. As a result, optical imaging can provide functional imaging—mapping of physiological parameters. By using multiwavelength measurement, one can simultaneously quantify concentrations of multiple chromophores of different colors, such as oxygenated and deoxygenated hemoglobin molecules in red blood cells. Such quantification of hemoglobin can provide functional imaging of the concentration and the oxygen saturation of hemoglobin—both parameters are related to angiogenesis and hypermetabolism (hallmarks of cancer)—as well as brain activities or injuries.[4,23,24] In addition, extrinsic optical absorption contrast agents can be used to provide molecular imaging of gene expressions or biomarkers.8–13

Challenges in optical imaging: optical diffraction and diffusion

High-resolution optical microscopy faces two fundamental challenges: diffraction and diffusion. Diffraction limits the spatial resolution, whereas diffusion limits the penetration. The resolution of optical microscopy has been improved beyond the diffraction limit recently.[25–27] This article focuses on breaking the diffusion limit.

Despite light diffusion due to tissue scattering, a quick experiment by transmitting flash light through the palm in the dark would prove the penetration capability of scattered light in biological tissue. Although the flash light is broadband, only red light transmits substantially. Unlike x-ray photons, optical photons do not cast a shadow of the bone. Such an observation is well-understood in biomedical optics. Because hemoglobin—the primary chromophore in biological tissue—absorbs light strongly in the green and blue spectral region, red light propagates further before being absorbed than shorter wavelength light. Further, strong light scattering by tissue components such as cell nuclei and mitochondria blurs any shadows of internal structures. In fact, a red photon may experience hundreds to thousands of scattering events before being absorbed. The reciprocal of the mean distance between equivalent isotropic scattering events—called transport mean free path—is on the order of 1 mm in the visible and near-infrared spectral range, around which photon propagation transitions from the ballistic regime into the diffusive regime.[28] Because optical focusing is ineffective in the diffusive regime, the transport mean free path is referred to as the soft depth limit for high-resolution optical imaging. Beyond the soft depth limit, no pure optical imaging technologies have been able to achieve high spatial resolution. Although scattering *per se* does not eliminate photons, tortuous elongated photon paths boost the chance of tissue absorption. Even diffuse photons are too few to be practically useful beyond a depth of ~50 mm, which is referred to as the hard depth limit for optical imaging.

Solutions to meet the challenges: photoacoustic tomography

PAT overcomes the soft depth limit and achieves deep imaging at high resolution. Ultrasonic scattering coefficient in tissue is 2–3 orders of magnitude less than the optical counterpart. As a result, PAT can provide high spatial resolution by detecting ultrasonic waves induced by diffuse photons. In most cases, the center frequency and the bandwidth of the ultrasonic detection system predominantly determine the spatial resolution; the greater they are, the better the spatial resolution is, but the worse the ultrasonic penetration becomes. Such scalability empowers multiscale imaging. It is worth mentioning that lower-frequency electromagnetic waves including microwaves and radiowaves have been adopted for photoacoustic excitation to overcome the optical hard depth limit.[29,30]

Ultrasound imaging can provide high spatial resolution although ultrasound images appear grainy owing to the speckle artifacts. The relative spatial resolution—defined as the ratio of the penetration limit to the depth resolution (i.e., the pixel count in the depth direction without artificial interpolation)—is more than 100, which is considered high enough to provide good-quality images. From ultrasound imaging, PAT inherits the attribute of high spatial resolution but rejects the trait of speckle formation. The speckle-free nature of PAT results from strong correlations among the photoacoustic waves from the absorbers because all initial photoacoustic pressure rises are positive. Consequently, prominent boundaries always build up in photoacoustic images and suppress the interior fluctuations.[31]

2. Fundamentals of PAT

Concept of PAT: optical excitation, ultrasonic detection, and image formation

Simply put, in PAT, light goes in and ultrasound comes out. For efficient ultrasound generation, a short-pulsed laser is the usual choice. The strength of the photoacoustic pressure depends on the optical energy deposition as well as the thermal and mechanical properties of the tissue. Because either unscattered or scattered photons can produce photoacoustic signals as long as photons are converted into heat, PAT can function in the optical diffusive regime. The image formation is essentially triangulation of the photoacoustic sources according to the time-of-flight signals recorded at multiple locations outside the tissue.[2,28]

Two major modes of PAT: focused scanning tomography and computed tomography

PAT manifests in two major modes. In the mode of focused scanning PAT, such as dark-field confocal photoacoustic microscopy (PAM),[32,33] a focused ultrasonic transducer is mechanically scanned.29 At each scanned position, the acoustic focusing yields lateral resolution while the acoustic time-of-flight provides axial resolution. In the mode of photoacoustic computed tomography, an array of unfocused ultrasonic transducers detects photoacoustic waves in parallel. Therefore, high frame rates—such as 50 Hz—can be attained.[3,4,21,34–46] However, an inverse reconstruction algorithm is required to reconstruct a tomographic image. The early reconstruction was based on the assumption that each ultrasonic transducer receives signals simultaneously from photoacoustic sources on a plane instead of a spherical surface,[21] which can be difficult to satisfy in practice. Later, various groups developed accurate reconstruction algorithms.[3] More recently, an exact closed-form reconstruction formula was found for three detection geometries: planar, cylindrical, and spherical configurations.[41] Interestingly, one may think of a focused ultrasonic transducer used in the first mode as an analog computer that performs approximately the inverse algorithm in the second mode. While hardware focusing does not present discretization artifacts, the focal position cannot be adjusted as readily as in photoacoustic computed tomography. As a result, the optimal lateral resolution is achievable only within the focal zone unless a virtual-detector-based synthetic aperture algorithm is used.

Contrast mechanisms of PAT: optical absorption and Grueneisen coefficient

PAT is exquisitely sensitive to optical absorption. The photoacoustic excitation converts a small change in optical absorption coefficient to an equal fractional change in ultrasound signal. For the same reason, PAT is also sensitive to any change in the Grueneisen coefficient—the conversion efficiency from optical energy deposition to pressure, which can also provide image contrast. In particular, the Grueneisen coefficient increases with the equilibrium temperature (e.g., ~5% per Kelvin in water), which enables PAT to image temperature with a sensitivity of 0.16 °C for monitoring of thermal therapy.[47–49]

Each mK of laser-induced temperature rise in soft tissue yields ~800 Pa initial pressure, which is on the order of the sensitivities of typical ultrasonic transducers. The conversion from temperature rise to pressure is related to two parameters: the volume expansion coefficient and the compressibility. It is fortunate that the two parameters conspire to enable PAT to be applicable in tissue with a safe temperature rise.

3. Multiscale photoacoustic microscopy

Dark-field confocal photoacoustic microscopy: 15 μm axial resolution, 3 mm depth

PAM can image optical-absorption contrast at depths beyond the optical transport mean free path with a ratio of penetration limit to depth resolution greater than 100 [Fig. 1(a)].[32,33] For ease of system operation, an optical fiber is used to deliver the excitation laser light, which is monitored by a photodiode for energy calibration. A conical lens is used to form a donut-shaped beam (i.e., dark field) so as to minimize the effect of surface photoacoustic signals on the deeper signals. The beam is then weakly focused into the tissue while the ultrasonic transducer focuses coaxially into the same region for confocal excitation and detection. The photoacoustic time-of-flight signal is recorded at each location of the ultrasonic transducer. By assuming the speed of sound to be 1.54 mm/μs, the time-of-flight is converted into depth, and consequently a 1D depth-resolved image (A-line) is formed. Linear or raster scanning over the tissue produces 2D or 3D tomographic images. Here, the broadband ultrasonic detector has a numerical aperture of 0.44 and a center frequency of 50 MHz. As a result, the lateral resolution, determined by the focal diameter of the ultrasonic transducer at the center frequency, measured ~45 μm. The axial resolution, determined by the ultrasonic bandwidth, measured ~15 μm. The maximum imaging depth, determined by the ultrasonic attenuation in tissue, measured >3 mm.[32,33] A representative PAM image is shown in Fig. 1(b).

Photoacoustic macroscopy: 144 μm axial resolution, 30 mm depth

The image resolution and the penetration limit are scalable with the ultrasonic frequency. For example, employing a 5-MHz ultrasonic transducer and an 804-nm near-infrared light source scaled the penetration to 30 mm, whereas the resolution is scaled up to 144 and 560 μm in the axial and lateral directions, respectively.[50] The near-infrared window is conducive for deep imaging because of the low hemoglobin absorption. Here, photoacoustic microscopy turns into macroscopy, which can potentially provide penetration up to the optical hard depth limit (~50 mm) at <1 mm resolution. Such a system can potentially image deep human tissue, such as the sentinel lymph node (SLN), which has an average depth of 12±5 mm in ultrasound images.[50] An *in vivo* image of a rat overlaid with additional tissue was acquired with this system [Fig. 1(c)], where the SLN accumulated injected dye through the lymphatics.[50] This imaging capability followed by needle biopsy can potentially transform SLN mapping—used for breast cancer staging—from a surgical procedure into a minimally invasive procedure.

Optical-resolution photoacoustic microscopy: 5 μm lateral resolution, 0.7 mm depth

The spatial resolution of the original PAM system can also be scaled down in dimension. Focusing light through an objective lens with a numerical aperture of 0.1 yields a 5 μm lateral

resolution, which is limited by the optical focal diameter. Such a resolution allows *in vivo* imaging of capillaries—the smallest blood vessels—as shown in Fig. 1(d), where single files of red blood cells are imaged.[51] While light delivery and ultrasonic detection are combined through a beam combiner in this work,[51] they were also combined earlier through a ring ultrasonic transducer.[52] If the numerical aperture is increased, sub-μm resolution can potentially be achieved. Of course, optical focusing is effective only within the soft depth limit.[28] Thus far, a 0.7 mm penetration has been achieved.

Multiscale photoacoustic microscopy/macroscopy: enabling systems biology research

Multiscale systems biology, recognized as an important future direction of biomedical sciences, needs the support of multiscale imaging *in vivo* with common signal origins. To understand the workings of a whole biological system, biological components spanning multiple spatial scales—subcellular organelles (sub-μm scale), through cells (μm), to organs (cm)—must be integrated. As demonstrated above, photoacoustic microscopy and macroscopy are uniquely positioned for such multiscale imaging with the same contrast mechanism—optical absorption.

Single-cell *in vivo* photoacoustic flow cytometry: melanoma detection

Photoacoustic sensing has recently been shown to detect single melanoma cells in lymph vessels *in vivo* in small animals.[53] This technology, coined *in vivo* photoacoustic flow cytometry, has potential for *in vivo* detection of circulating tumor cells in humans. Cells flowing through a lymph valve are naturally focused into a single file, which facilitates single cell detection in a lymph vessel. The lymph transparency presents low background and consequently facilitates high-sensitivity detection. Melanin in the melanoma cells provides high optical absorption for photoacoustic detection without the use of exogenous labeling, which can be toxic. Nonetheless, exogenous contrast agents can be used to provide molecular specificity for targeted biomarkers.[53] Several optical wavelengths can be used to detect multiple types of cells of different characteristic optical absorption spectra. Toward human applications, it was suggested that superficial lymphatics in the leg be first targeted.[54] The concept can also be applied to blood vessels although background due to erythrocytes can compete with signals from other absorbers.[55–58] Currently, the technology is limited to non-imaging sensing; however, PAM can be explored for imaging.

4. Photoacoustic computed tomography

Circular-view computed tomography: 1D circular scan or ring array

In circular-view photoacoustic computed tomography, ultrasonic detection follows a ring.[4,59,60] A pulsed laser beam is expanded to illuminate the object. An ultrasonic transducer scans around the object in a circle to acquire the photoacoustic data. An inverse algorithm then converts the photoacoustic data to the initial photoacoustic pressure distribution, which is an image of the cross section containing the scanned circle. Representative functional images are shown in Fig. 2(a).[4] The ultrasonic transducer has a broad bandwidth centered at 3.5 MHz, yielding an in-plane resolution of ~200 μm. The out-of-plane resolution, determined by the cylindrical focusing of the transducer, is ~1 mm. To accelerate the imaging speed, an array of ultrasonic transducers in a ring has been adopted.[61]

Planar-view computed tomography: Fabry-Perot detection array

In planar-view photoacoustic computed tomography, ultrasonic detection follows a plane.[34] Optical interferometry, instead of the piezoelectric effect, can be used to sense the ultrasonic displacement[62–65] or pressure.[66,67] When a solid planar Fabry-Perot interferometer was constructed,[67,68] a dielectric or polymer spacer was sandwiched between a pair of mirrors. A focused laser beam was optically scanned across the surface of the interferometer. The detected

power fluctuation of the reflected laser beam was converted to the optical thickness of the interferometer, which was further converted to pressure. Then, an inverse algorithm was used to reconstruct a photoacoustic image [Fig. 2(b)].[68,69]

Optical detection offers primarily three advantages.[67] First, the optical detector can be made optically transparent, facilitating light delivery to the object for full-field imaging. Second, the spatial sampling frequency can be increased without sacrificing the sensitivity, allowing high-resolution imaging. Sensitivities of tens of Pascals have been achieved at 20-MHz bandwidth.[67] Such sensitivities are comparable with those of 1-mm-diameter piezoelectric receivers and better than those of smaller-diameter ones. Third, the frequency response can be stretched to low frequencies, potentially enabling the detection of the interior of a large heterogeneity. Presently, the technology is limited by the system complexity and the read-out speed.

Spherical-view computed tomography: rotation of object and detection by arc array

In spherical-view photoacoustic computed tomography, ultrasonic detection follows a truncated spherical surface.[70] In a recently constructed small-animal whole-body photoacoustic tomography system,[71] the animal, immersed in coupling liquid, is rotated inside a virtual spherical surface, on which a concave arc-shaped array of 64 piezo-composite ultrasonic transducers is situated. Two expanded counter-propagating laser beams illuminate the small animal orthogonally to the plane of the array. At 755 nm wavelength, the internal organs of a nude mouse were imaged [Fig. 2(c)].[71]

Linear-view computed tomography: 1D linear ultrasonic array

In linear-view photoacoustic computed tomography, ultrasonic detection follows a line.[72–77] Linear ultrasound arrays in medical ultrasound imaging systems can be leveraged. The ultrasound probes are typically handheld and can therefore adapt to various anatomical sites conveniently. In ultrasound imaging, a subset of the array elements is switched on at a time for ultrasound transmission and detection. Shifting the selection of the subset across the array forms a two-dimensional image. In PAT, the entire array can receive ultrasonic signals simultaneously because photoacoustic excitation usually covers a large volume. Naturally, ultrasound and photoacoustic images can be displayed side-by-side to present complementary contrasts.

Computed tomography based on linear or planar ultrasonic detectors

Photoacoustic computed tomography can be based on linear or planar ultrasonic transducers instead of point detectors.[40,78–80] In this case, the detected signals represent an integration of pressure over cylindrical or planar surfaces with varying distances to each transducer. Planar ultrasonic transduction is of particular interest for primarily two reasons. First, the forward problem represents a standard Radon transformation used in x-ray computed tomography. Therefore, the associated inverse algorithms can be used directly for PAT. Second, the spatial resolution is limited only by the ultrasonic bandwidth. In conventional photoacoustic computed tomography, point ultrasonic detectors are approximated by finite-size detectors, resulting in a tradeoff between the detection sensitivity and the lateral resolution. If the detectors are too small, the sensitivity is compromised; if too large, the resolution becomes poor. Such a compromise is devoid in PAT based on planar ultrasonic transducers.

Photoacoustic breast imaging

PAT lends itself to breast imaging. Breast tissue has relatively homogeneous (~±5%) speed of sound, and breast tumors tend to present higher total blood concentrations and lower oxygen saturations of hemoglobin than surrounding tissues. Figure 3(a) shows an *in vivo* photoacoustic image of a human breast,[81] where the ultrasonic detection follows an arc.[37] The imaged lesion

measured ~18 mm and centered at 23 mm deep from the laser-illumination surface; it was confirmed by biopsy to be an invasive carcinoma. Figure 3(b) shows another *in vivo* photoacoustic image of a human breast,82 where the ultrasonic detection follows a plane.[83] The lesion was identified as a ring-shaped structure having an average optical absorption contrast of 1.6 relative to the background. The lesion was estimated to be 30 mm in diameter, which matched the pathologically estimated size (26 mm).

5. Photoacoustic molecular imaging

Small-molecule contrast: biomarkers imaged *in vivo*

PAT is well suited for molecular imaging. While functional imaging is based on endogenous contrast, molecular imaging is based on exogenous contrast—which essentially stains invisible biomarkers *in vivo*. Functional imaging maps physiological activities usually at the tissue or organ level, whereas molecular imaging measures biological and pathophysiological processes at the molecular level. Simultaneous functional and molecular PAT of glioblastoma brain tumors was demonstrated in live mice.[13] A small-molecule organic dye conjugated with a cyclopeptide serves as the molecular imaging probe to target biomarker $\alpha_v\beta_3$ integrin, which tends to over-express in angiogenesis. The functional image shows tumor hypoxia, whereas the molecular image shows tumor over-expression of integrin.

Nanoparticle contrast: biomarkers imaged

PAT can track various nanoparticles, such as metallic nanoshells[84], nanorods[10,85–89], nanocages[90], carbon nanotubes[9], and dye-embedded nanoparticles[91]. The large optical absorption cross sections of nanoparticles[92] provide excellent contrast for PAT. Unlike small-molecule organic dyes, nanoparticles resist chemical or thermal denaturation and photobleaching. However, further toxicity studies toward human applications are needed.

The surfaces of gold nanoparticles exhibit good biocompatibility and can accommodate functionalities by conjugating with targeting peptides or antibodies.[11,87,93] So far, biomarkers targeted in PAT include EGFR[11], HER-2[87] and CXCR-4[93], which have a propensity to overexpress in cancers such as the breast cancer, as well as ICAM-1 in inflammatory responses.[88] In metallic nanoparticles, the optical absorption is based on surface plasmon resonance, and the peak absorption wavelength can be tuned throughout the visible and near-infrared spectral region by varying the physical dimensions.

Dye-embedded nanoparticles can also function as an effective contrast agent.[91] Indocyanine green (ICG) is an organic dye that has been approved for human use. It has strong optical absorption around the 800-nm near-infrared wavelength. Although free-form ICG has been demonstrated to enhance photoacoustic contrast *in vivo*,[94] the half-life of ICG in the blood stream is only several minutes, limiting the time window for sustained monitoring. Encapsulation of ICG in nanoparticles increases the circulation time significantly.[91] In addition, encapsulation provides surfaces for adding functionalities, increases the dye concentration for greater optical absorption, and shields the dye molecules from destabilizing effects due to the biological environment. ICG-embedded nanoparticles conjugated with HER-2 antibodies have been shown to target breast cancer and prostate cancer cells *in vitro*.[91]

Reporter gene contrast: gene expression imaged *in vivo*

Molecular PAT of the lacZ reporter gene was demonstrated in living small animals.[8] Reporter gene imaging, a form of molecular imaging, can facilitate understanding the nature of gene expression during *in vivo* development and pathogenesis. While conventional reporter gene imaging is based on fluorescent proteins such as the well-known green fluorescent protein,

photoacoustic reporter gene imaging is based on optical absorption that is converted into heat. The lacZ gene—one of the most widely used reporter genes—encodes β-galactosidase. A sensitive chromogenic assay with X-gal—an optically transparent substrate—yields a stable dark blue product, which serves as an optical absorption contrast agent for PAT. Because the absorption of the blue product peaks around 650 nm, multi-millimeter penetration can be achieved. However, if multi-centimeter penetration is desired, new reporter genes that produce gene-expression products absorbing in the near-infrared spectral region need to be developed. By providing high spatial resolution at depths beyond the optical transport mean free path *in vivo*, PAT is expected to become a complementary tool to conventional optical imaging of reporter genes.

Sensitivity to contrast agent

The sensitivity of PAT is competitive among the various molecular imaging modalities although such a comparison depends on many parameters as well as the biomedical applications.[95] When intrinsic biological contrasts due to such as red blood cells or melanoma cells are sensed, single-cell sensitivity has been achieved.[51,55] When extrinsic small-molecule contrast agents are imaged, PAT can provide a sensitivity of the order of ~10 nmol/L or ~fmol/voxel at ~0.3 mm resolution.[13,96] Pure optical fluorescence imaging can provide a sensitivity of the order of ~nmol/L or ~fmol/voxel at ~1 mm resolution,[97] where the resolution is worse than that of PAT and the sensitivity is slightly better. Nuclear imaging such as PET can provide a sensitivity of the order of ~pmol/L or ~0.1 fmol/voxel at ~3 mm resolution, where the resolution is much worse than that of PAT and the sensitivity is better.[98,99] However, the sensitivity of PAT can be improved potentially by increasing parameters such as the local optical fluence, the optical absorption cross section of the contrast agent, the number of signals for averaging, and the voxel size. For example, when extrinsic nanoshell contrast agents are imaged, PAT can provide a sensitivity of the order of ~10 pmol/L or ~0.0001 fmol/voxel at ~0.06 mm resolution.[84] Because different modalities have dissimilar imaging capabilities, the sensitivity should not be the only parameter governing the selection of a tool for a particular application. In additional, nuclear imaging uses ionizing radiation, whereas PAT and optical fluorescence imaging use nonionizing radiation.

6. Limitations of PAT and future outlook

PAT has limitations as does any imaging technology. First, optical attenuation limits the penetration to ~5 cm when <1 mm resolution is desired in actual tissue.[81,100,101] However, microwaves or radiowaves can be used for deeper excitation although the contrast origins differ. Second, ultrasound sustains strong reflection from gas–liquid or gas–solid interfaces due to the strong mismatch of acoustic impedances. Therefore, ultrasound signals cannot penetrate through gas cavities or lung tissues efficiently. For the same reason, ultrasonic detection requires direct contact between the ultrasonic transducers and the biological tissue. Usually, ultrasound coupling gel is applied to the tissue surface to avoid intervening air cavities. The development of noncontact optical detection of acoustic displacement can potentially overcome this problem.[62–65] Third, ultrasound suffers significant attenuation and phase distortion in thick bones such as the human skull. Fortunately, unlike pulse-echo ultrasound imaging, PAT involves only one-way ultrasound attenuation through the skull. Sufficiently strong photoacoustic signals have been observed through Rhesus monkey skulls.[102,103] The remaining challenge is to compensate for the phase distortion due to the skull.

The research field on PAT has gained significant momentum recently. The number of research articles on PAT has more than tripled since year 2003.[104] PAT is expected to find broad applications in both biology and medicine. In the author's opinion, the following *in vivo* applications hold particular promises and may come to fruition in the near future: melanoma detection,[32,53,56,58] intravascular catheter imaging,[105–107] endoscopic imaging, simultaneous

functional and molecular imaging,[13] reporter gene imaging,[8] sentinel lymph node mapping,[50,59] breast imaging,[81,82,108–110] and multiscale imaging.

Acknowledgments

The author acknowledges the support by the National Institutes of Health Grants R01 EB000712, R01 NS046214, R01 EB008085, and U54 CA136398. Thanks to Song Hu for providing Fig. 1(d).

References

1. Oraevsky, AA.; Karabutov, AA. Biomedical Photonics Handbook. Vo-Dinh, T., editor. Vol. PM125. CRC Press; 2003. p. 3401-3434.Ch. 34
2. Xu MH, Wang LV. Photoacoustic imaging in biomedicine. Rev Sci Instrum 2006;77:41101–41122.
3. Wang, LV., editor. Photoacoustic Imaging and Spectroscopy. CRC; 2009.
4. Wang XD, et al. Noninvasive laser-induced photoacoustic tomography for structural and functional in vivo imaging of the brain. Nat Biotechnol 2003;21:803–806. [PubMed: 12808463]
5. Siphanto RI, et al. Serial noninvasive photoacoustic imaging of neovascularization in tumor angiogenesis. Opt Express 2005;13:89–95. [PubMed: 19488331]
6. Laufer J, Delpy D, Elwell C, Beard P. Quantitative spatially resolved measurement of tissue chromophore concentrations using photoacoustic spectroscopy: application to the measurement of blood oxygenation and haemoglobin concentration. Phys Med Biol 2007;52:141–168. [PubMed: 17183133]
7. Yang S, Xing D, Zhou Q, Xiang L, Lao Y. Functional imaging of cerebrovascular activities in small animals using high-resolution photoacoustic tomography. Med Phys 2007;34:3294–3301. [PubMed: 17879793]
8. Li L, Zemp RJ, Lungu G, Stoica G, Wang LV. Photoacoustic imaging of lacZ gene expression in vivo. J Biomed Opt 2007;12:020504. [PubMed: 17477703]
9. De La Zerda A, et al. Carbon nanotubes as photoacoustic molecular imaging agents in living mice. Nat Nanotechnol 2008;3:557–562. [PubMed: 18772918]
10. Copland JA, et al. Bioconjugated gold nanoparticles as a molecular based contrast agent: Implications for imaging of deep tumors using optoacoustic tomography. Mol Imag Biol 2004;6:341–349.
11. Mallidi S, Larson T, Aaron J, Sokolov K, Emelianov S. Molecular specific optoacoustic imaging with plasmonic nanoparticles. Opt Express 2007;15:6583–6588. [PubMed: 19546967]
12. Razansky D, Ntziachristos V. Hybrid photoacoustic fluorescence molecular tomography using finite-element-based inversion. Med Phys 2007;34:4293–4301. [PubMed: 18072494]
13. Li ML, et al. Simultaneous molecular and hypoxia imaging of brain tumors in vivo using spectroscopic photoacoustic tomography. Proc IEEE 2008;96:481–489.
14. Bell AG. On the production and reproduction of sound by light. Am J Sci 1880;20:305–324.
15. Bowen, T. Radiation-induced thermoacoustic imaging. 1983. United States patent 4,385,634
16. Oraevsky AA, Jacques SL, Tittel FK. Determination of tissue optical properties by time-resolved detection of laser-induced stress waves. Proc SPIE 1993;1882:86–101.
17. Oraevsky AA, Jacques SL, Esenaliev RO, Tittel FK. Laser-based optoacoustic imaging in biological tissues. Proc SPIE 1994;2134A:122–128.
18. Kruger RA. Photoacoustic Ultrasound. Med Phys 1994;21:127–131. [PubMed: 8164577]
19. Kruger RA, Liu PY. Photoacoustic Ultrasound - Pulse Production and Detection in 0.5-Percent Liposyn. Med Phys 1994;21:1179–1184. [PubMed: 7968851]
20. Oraevsky AA, Esenaliev RO, Jacques SL, Thomsen SL, Tittel FK. Lateral and z-axial resolution in laser optoacoustic imaging with ultrasonic transducers. Proc SPIE 1995;2389:198–208.
21. Kruger RA, Liu PY, Fang YR, Appledorn CR. Photoacoustic Ultrasound (PAUS) - Reconstruction Tomography. Med Phys 1995;22:1605–1609. [PubMed: 8551984]
22. Ku G, Wang LV. Scanning thermoacoustic tomography in biological tissue. Med Phys 2000;27:1195–1202. [PubMed: 10841427]

23. Yang SH, et al. Noninvasive monitoring of traumatic brain injury and post-traumatic rehabilitation with laser-induced photoacoustic imaging. Appl Phys Lett 2007;90:243902.
24. Zhang QZ, et al. Non-invasive imaging of epileptic seizures in vivo using photoacoustic tomography. Phys Med Biol 2008;53:1921–1931. [PubMed: 18364547]
25. Betzig E, et al. Imaging intracellular fluorescent proteins at nanometer resolution. Science 2006;313:1642–1645. [PubMed: 16902090]
26. Hell SW. Far-field optical nanoscopy. Science 2007;316:1153–1158. [PubMed: 17525330]
27. Huang B, Wang WQ, Bates M, Zhuang XW. Three-dimensional super-resolution imaging by stochastic optical reconstruction microscopy. Science 2008;319:810–813. [PubMed: 18174397]
28. Wang, LV.; Wu, H. Biomedical Optics: Principles and Imaging. Wiley; 2007.
29. Wang LV, Zhao XM, Sun HT, Ku G. Microwave-induced acoustic imaging of biological tissues. Rev Sci Instrum 1999;70:3744–3748.
30. Kruger RA, Reinecke DR, Kruger GA. Thermoacoustic computed tomography-technical considerations. Med Phys 1999;26:1832–1837. [PubMed: 10505871]
31. Guo Z, Li L, Wang LV. The speckle-free nature of photoacoustic tomography. Proc SPIE 2009;7177:71772J.
32. Zhang HF, Maslov K, Stoica G, Wang LV. Functional photoacoustic microscopy for high-resolution and noninvasive in vivo imaging. Nat Biotechnol 2006;24:848–851. [PubMed: 16823374]
33. Zhang HF, Maslov K, Wang LV. In vivo imaging of subcutaneous structures using functional photoacoustic microscopy. Nat Protoc 2007;2:797–804. [PubMed: 17446879]
34. Hoelen CGA, de Mul FFM, Pongers R, Dekker A. Three-dimensional photoacoustic imaging of blood vessels in tissue. Opt Lett 1998;23:648–650. [PubMed: 18084605]
35. Kostli KP, et al. Optoacoustic imaging using a three-dimensional reconstruction algorithm. IEEE J Sel Top Quantum Electron 2001;7:918–923.
36. Paltauf G, Viator JA, Prahl SA, Jacques SL. Iterative reconstruction algorithm for optoacoustic imaging. J Acoust Soc Am 2002;112:1536–1544. [PubMed: 12398460]
37. Andreev VG, Karabutov AA, Oraevsky AA. Detection of ultrawide-band ultrasound pulses in optoacoustic tomography. IEEE Trans Ultrason Ferroelectr Freq Control 2003;50:1383–1390. [PubMed: 14609079]
38. Finch D, Patch SK, Rakesh. Determining a function from its mean values over a family of spheres. SIAM J Math Anal 2003;35:1213–1240.
39. Kostli KP, Beard PC. Two-dimensional photoacoustic imaging by use of Fourier-transform image reconstruction and a detector with an anisotropic response. Appl Opt 2003;42:1899–1908. [PubMed: 12683772]
40. Haltmeier M, Scherzer O, Burgholzer P, Paltauf G. Thermoacoustic computed tomography with large planar receivers. Inverse Probl 2004;20:1663–1673.
41. Xu MH, Wang LV. Universal back-projection algorithm for photoacoustic computed tomography. Phys Rev E 2005;71:016706.
42. Cox BT, Beard PC. Fast calculation of pulsed photoacoustic fields in fluids using k-space methods. J Acoust Soc Am 2005;117:3616–3627. [PubMed: 16018465]
43. Cox BT, Arridge SR, Kostli KP, Beard PC. Two-dimensional quantitative photoacoustic image reconstruction of absorption distributions in scattering media by use of a simple iterative method. Appl Opt 2006;45:1866–1875. [PubMed: 16572706]
44. Anastasio MA, Zhang J, Modgil D, La Riviere PJ. Application of inverse source concepts to photoacoustic tomography. Inverse Probl 2007;23:S21–S35.
45. Hoelen CGA, de Mul FFM. Image reconstruction for photoacoustic scanning of tissue structures. Appl Opt 2000;39:5872–5883. [PubMed: 18354591]
46. Kostli KP, Frenz M, Bebie H, Weber HP. Temporal backward projection of optoacoustic pressure transients using Fourier transform methods. Phys Med Biol 2001;46:1863–1872. [PubMed: 11474930]
47. Larina IV, Larin KV, Esenaliev RO. Real-time optoacoustic monitoring of temperature in tissues. J Phys D: Appl Phys 2005;38:2633–2639.

48. Sethuraman S, Aglyamov SR, Smalling RW, Emelianov SY. Remote temperature estimation in intravascular photoacoustic imaging. Ultrasound Med Biol 2008;34:299–308. [PubMed: 17935861]
49. Shah J, et al. Photoacoustic imaging and temperature measurement for photothermal cancer therapy. J Biomed Opt 2008;13:034024. [PubMed: 18601569]
50. Song KH, Stein EW, Margenthaler JA, Wang LV. Noninvasive photoacoustic identification of sentinel lymph nodes containing methylene blue in vivo in a rat model. J Biomed Opt 2008;13:054033. [PubMed: 19021413]
51. Maslov K, Zhang HF, Hu S, Wang LV. Optical-resolution photoacoustic microscopy for in vivo imaging of single capillaries. Opt Lett 2008;33:929–931. [PubMed: 18451942]
52. Savateeva EV, et al. Noninvasive detection and staging of oral cancer in vivo with confocal optoacoustic tomography. Proc SPIE 2000;3916:55–66.
53. Galanzha EI, Shashkov EV, Tuchin VV, Zharov VP. In vivo multispectral, multiparameter, photoacoustic lymph flow cytometry with natural cell focusing, label-free detection and multicolor nanoparticle probes. Cytometry A 2008;73A:884–894. [PubMed: 18677768]
54. Olszewski W, Tarnok A. Photoacoustic listening of cells in lymphatics: Research art or novel clinical noninvasive lymph test. Cytometry A 2008;73A:1111–1113. [PubMed: 18985726]
55. Zharov VP, Galanzha EI, Shashkov EV, Khlebtsov NG, Tuchin VV. In vivo photoacoustic flow cytometry for monitoring of circulating single cancer cells and contrast agents. Opt Lett 2006;31:3623–3625. [PubMed: 17130924]
56. Weight RM, Viator JA, Dale PS, Caldwell CW, Lisle AE. Photoacoustic detection of metastatic melanoma cells in the human circulatory system. Opt Lett 2006;31:2998–3000. [PubMed: 17001379]
57. Zharov VP, et al. Photoacoustic flow cytometry: principle and application for real-time detection of circulating single nanoparticles, pathogens, and contrast dyes in vivo. J Biomed Opt 2007;12:051503. [PubMed: 17994867]
58. Holan SH, Viator JA. Automated wavelet denoising of photoacoustic signals for circulating melanoma cell detection and burn image reconstruction. Phys Med Biol 2008;53:N227–N236. [PubMed: 18495977]
59. Ambartsounnian G, Kuchment P. On the injectivity of the circular Radon transform. Inverse Probl 2005;21:473–485.
60. Haltmeier M, Scherzer O, Burgholzer P, Nustero R, Paltauf G. Thermoacoustic tomography and the circular radon transform: Exact inversion formula. Math Models Methods Appl Sci 2007;17:635–655.
61. Gamelin J, et al. Curved array photoacoustic tomographic system for small animal imaging. J Biomed Opt 2008;13:024007. [PubMed: 18465970]
62. Hamilton JD, O'Donnell M. High frequency ultrasound imaging with optical arrays. IEEE Trans Ultrason Ferroelectr Freq Control 1998;45:216–235. [PubMed: 18244174]
63. Payne BP, Venugopalan V, Mikc BB, Nishioka NS. Optoacoustic tomography using time resolved interferometric detection of surface displacement. J Biomed Opt 2003;8:273–280. [PubMed: 12683854]
64. Carp SA, Guerra A, Duque SQ, Venugopalan V. Optoacoustic imaging using interferometric measurement of surface displacement. Appl Phys Lett 2004;85:5772–5774.
65. Carp SA, Venugopalan V. Optoacoustic imaging based on the interferometric measurement of surface displacement. J Biomed Opt 2007;12:064001. [PubMed: 18163817]
66. Beard PC, Perennes F, Mills TN. Transduction mechanisms of the Fabry-Perot polymer film sensing concept for wideband ultrasound detection. IEEE Trans Ultrason Ferroelectr Freq Control 1999;46:1575–1582. [PubMed: 18244356]
67. Zhang E, Laufer J, Beard P. Backward-mode multiwavelength photoacoustic scanner using a planar Fabry-Perot polymer film ultrasound sensor for high-resolution three-dimensional imaging of biological tissues. Appl Opt 2008;47:561–577. [PubMed: 18239717]
68. Laufer JG, Zhang EZ, Raivich G, Beard PC. Three dimensional noninvasive imaging of the vasculature in the mouse brain using a high resolution photoacoustic scanner. Appl Opt 2009;48:D299–D306. [PubMed: 19340121]
69. Zhang EZ, Laufer JG, Pedley RB, Beard PC. In vivo high-resolution 3D photoacoustic imaging of superficial vascular anatomy. Phys Med Biol 2009;54:1035–1046. [PubMed: 19168938]

70. Kruger RA, Kiser WL, Reinecke DR, Kruger GA, Miller KD. Thermoacoustic molecular imaging of small animals. Mol Imaging 2003;2:113–123. [PubMed: 12964308]
71. Brecht HP, et al. Optoacoustic 3D whole-body tomography: experiments in nude mice. Proc SPIE 2009;7177:71770E.
72. Kruger RA, Kiser WL, Reinecke DR, Kruger GA. Thermoacoustic computed tomography using a conventional linear transducer array. Med Phys 2003;30:856–860. [PubMed: 12772993]
73. Zeng YG, Xing D, Wang Y, Yin BZ, Chen Q. Photoacoustic and ultrasonic coimage with a linear transducer array. Opt Lett 2004;29:1760–1762. [PubMed: 15352361]
74. Yin BZ, et al. Fast photoacoustic imaging system based on 320-element linear transducer array. Phys Med Biol 2004;49:1339–1346. [PubMed: 15128209]
75. Niederhauser JJ, Jaeger M, Lemor R, Weber P, Frenz M. Combined ultrasound and optoacoustic system for real-time high-contrast vascular imaging in vivo. IEEE Trans Med Imaging 2005;24:436–440. [PubMed: 15822801]
76. Yang DW, Xing D, Yang SH, Xiang LZ. Fast full-view photoacoustic imaging by combined scanning with a linear transducer array. Opt Express 2007;15:15566–15575. [PubMed: 19550843]
77. Nie LM, Xing D, Yang DW, Zeng LM, Zhou Q. Detection of foreign body using fast thermoacoustic tomography with a multielement linear transducer array. Appl Phys Lett 2007;90:174109.
78. Burgholzer P, Hofer C, Paltauf G, Haltmeier M, Scherzer O. Thermoacoustic tomography with integrating area and line detectors. IEEE Trans Ultrason Ferroelectr Freq Control 2005;52:1577–1583. [PubMed: 16285456]
79. Burgholzer P, Bauer-Marschallinger J, Grun H, Haltmeier M, Paltauf G. Temporal back-projection algorithms for photoacoustic tomography with integrating line detectors. Inverse Probl 2007;23:65–80.
80. Paltauf G, Nuster R, Haltmeier M, Burgholzer P. Experimental evaluation of reconstruction algorithms for limited view photoacoustic tomography with line detectors. Inverse Probl 2007;23:S81–S94.
81. Ermilov SA, et al. Laser optoacoustic imaging system for detection of breast cancer. J Biomed Opt 2009;14:024007. [PubMed: 19405737]
82. Manohar S, et al. Initial results of in vivo non-invasive cancer imaging in the human breast using near-infrared photoacoustics. Opt Express 2007;15:12277–12285. [PubMed: 19547596]
83. Manohar S, Kharine A, van Hespen JCG, Steenbergen W, van Leeuwen TG. The Twente Photoacoustic Mammoscope: system overview and performance. Phys Med Biol 2005;50:2543–2557. [PubMed: 15901953]
84. Wang YW, et al. Photoacoustic tomography of a nanoshell contrast agent in the in vivo rat brain. Nano Lett 2004;4:1689–1692.
85. Li PC, et al. Photoacoustic flow measurements by use of laser-induced shape transitions of gold nanorods. Opt Lett 2005;30:3341–3343. [PubMed: 16389825]
86. Eghtedari M, et al. High sensitivity of in vivo detection of gold nanorods using a laser optoacoustic imaging system. Nano Lett 2007;7:1914–1918. [PubMed: 17570730]
87. Agarwal A, et al. Targeted gold nanorod contrast agent for prostate cancer detection by photoacoustic imaging. J Appl Phys 2007;102:064701.
88. Kim K, et al. Photoacoustic imaging of early inflammatory response using gold nanorods. Appl Phys Lett 2007;90:223901.
89. Chamberland DL, et al. Photoacoustic tomography of joints aided by an Etanercept-conjugated gold nanoparticle contrast agent - an ex vivo preliminary rat study. Nanotechnology 2008;19:095101.
90. Yang XM, Skrabalak SE, Li ZY, Xia YN, Wang LV. Photoacoustic tomography of a rat cerebral cortex in vivo with au nanocages as an optical contrast agent. Nano Lett 2007;7:3798–3802. [PubMed: 18020475]
91. Kim G, et al. Indocyanine-green-embedded PEBBLEs as a contrast agent for photoacoustic imaging. J Biomed Opt 2007;12:044020. [PubMed: 17867824]
92. Hu M, et al. Gold nanostructures: engineering their plasmonic properties for biomedical applications. Chem Soc Rev 2006;35:1084–1094. [PubMed: 17057837]

93. Li PC, et al. Photoacoustic imaging of multiple targets using gold nanorods. IEEE Trans Ultrason Ferroelectr Freq Control 2007;54:1642–1647. [PubMed: 17703668]
94. Wang XD, et al. Noninvasive photoacoustic angiography of animal brains in vivo with near-infrared light and an optical contrast agent. Opt Lett 2004;29:730–732. [PubMed: 15072373]
95. Razansky D, Baeten J, Ntziachristos V. Sensitivity of molecular target detection by multispectral optoacoustic tomography (MSOT). Med Phys 2009;36:939–945. [PubMed: 19378754]
96. Razansky D, Vinegoni C, Ntziachristos V. Multispectral photoacoustic imaging of fluorochromes in small animals. Opt Lett 2007;32:2891–2893. [PubMed: 17909608]
97. Ntziachristos V, Ripoll J, Wang LHV, Weissleder R. Looking and listening to light: the evolution of whole-body photonic imaging. Nat Biotechnol 2005;23:313–320. [PubMed: 15765087]
98. Phelps ME. PET - A biological imaging technique. Neurochem Res 1991;16:929–940. [PubMed: 1784338]
99. MacLaren DC, et al. PET imaging of transgene expression. Biol Psychiatry 2000;48:337–348. [PubMed: 10978717]
100. Esenaliev RO, Karabutov AA, Oraevsky AA. Sensitivity of laser opto-acoustic imaging in detection of small deeply embedded tumors. IEEE J Sel Top Quantum Electron 1999;5:981–988.
101. Ku G, Wang LV. Deeply penetrating photoacoustic tomography in biological tissues enhanced with an optical contrast agent. Opt Lett 2005;30:507–509. [PubMed: 15789718]
102. Xu Y, Wang LV. Rhesus monkey brain imaging through intact skull with thermoacoustic tomography. IEEE Trans Ultrason Ferroelectr Freq Control 2006;53:542–548. [PubMed: 16555762]
103. Yang XM, Wang LV. Monkey brain cortex imaging by photoacoustic tomography. J Biomed Opt 2008;13:044009. [PubMed: 19021337]
104. Source: Science Citation Index. Search criteria: Topic=((photoacoustic or optoacoustic) and (imaging or tomography or microscopy)) AND Document Type=(Article).
105. Sethuraman S, Amirian JH, Litovsky SH, Smalling RW, Emelianov SY. Ex vivo characterization of atherosclerosis using intravascular photoacoustic imaging. Opt Express 2007;15:16657–16666. [PubMed: 19550952]
106. Sethuraman S, Aglyamov SR, Amirian JH, Smalling RW, Emelianov SY. Intravascular photoacoustic imaging using an IVUS imaging catheter. IEEE Trans Ultrason Ferroelectr Freq Control 2007;54:978–986. [PubMed: 17523562]
107. Sethuraman S, Amirian JH, Litovsky SH, Smalling RW, Emelianov SY. Spectroscopic intravascular photoacoustic imaging to differentiate atherosclerotic plaques. Opt Express 2008;16:3362–3367. [PubMed: 18542427]
108. Oraevsky AA, et al. Initial clinical evaluation of laser optoacoustic imaging system for diagnostic imaging of breast cancer. Breast Cancer Res Treat 2007;106:S47–S47.
109. Manohar S, Kharine A, van Hespen JCG, Steenbergen W, van Leeuwen TG. Photoacoustic mammography laboratory prototype: imaging of breast tissue phantoms. J Biomed Opt 2004;9:1172–1181. [PubMed: 15568937]
110. Kruger RA, et al. Breast cancer in vivo: Contrast enhancement with thermoacoustic CT at 434 MHz - Feasibility study. Radiology 2000;216:279–283. [PubMed: 10887262]

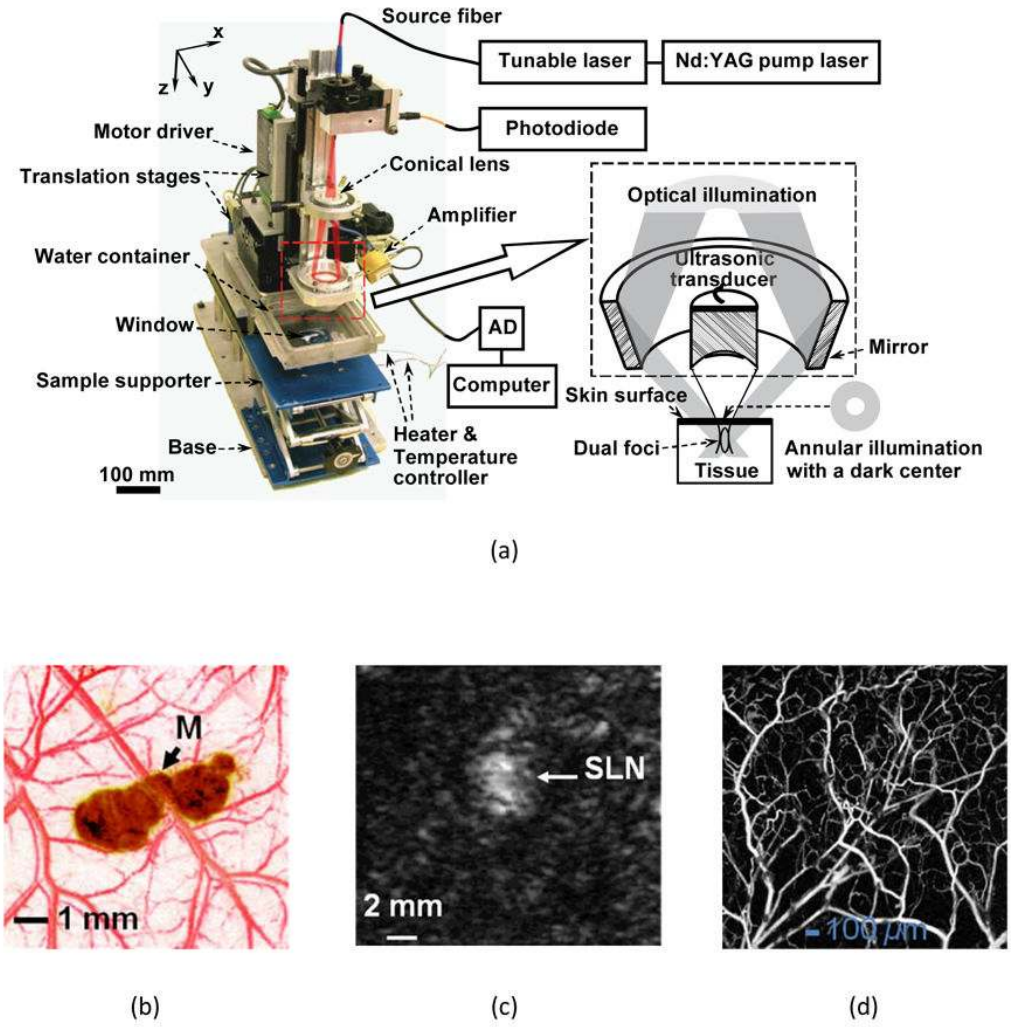

Figure 1. Multiscale scanning photoacoustic imaging of small animals *in vivo*

(a) Annotated photograph of the dark-field confocal photoacoustic microscope.32 (b) Photoacoustic image of a melanoma and blood vessels acquired with a 50-MHz photoacoustic microscope.32 M: melanoma. Axial resolution: 15 μm. Penetration limit: 3 mm. (c) Photoacoustic image of a sentinel lymph node (SLN) 18 mm below the laser-illumination surface acquired with a 5-MHz photoacoustic macroscope.50 Axial resolution: 144 μm. Penetration limit: 30 mm. (d) Photoacoustic image of the vasculature, including capillaries, acquired with an optical-resolution photoacoustic microscope.51 Lateral resolution: 5 μm. Penetration limit: 0.7 mm.

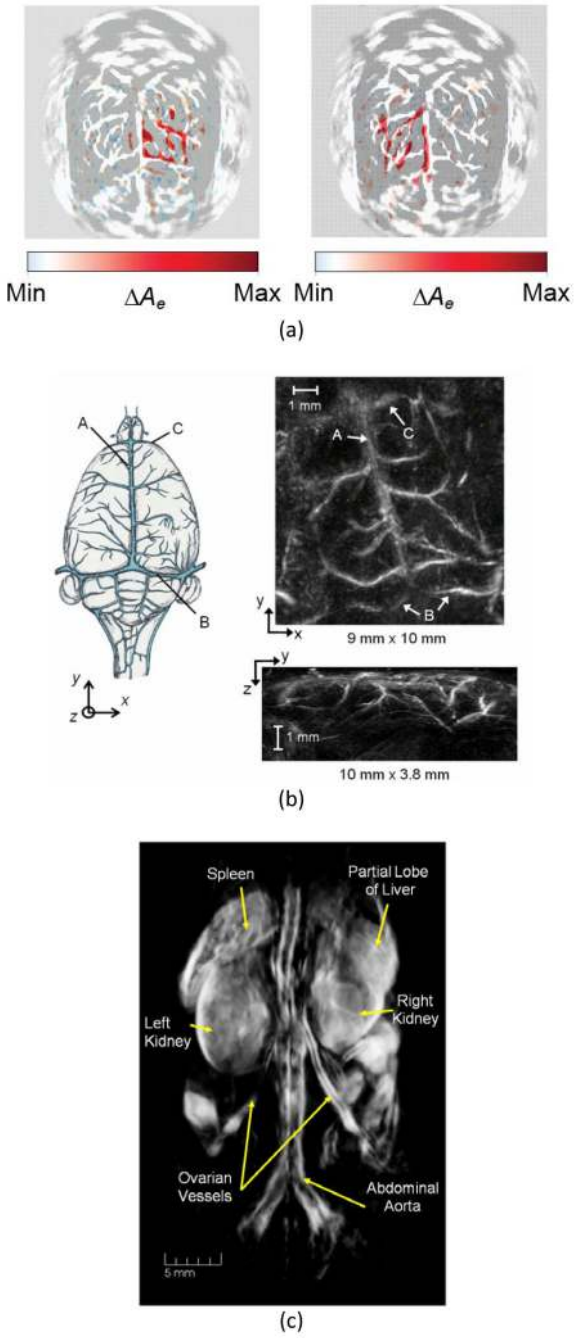

Figure 2. Non-invasive photoacoustic computed tomography of small animals

(a) Functional images of a rat brain acquired *in vivo* with left- and right-side whisker stimulations, respectively.[4] Color: differential absorption ΔA_e due to brain activation. Gray: structure of the cortex. Field of view: 20 × 20 mm. (b) Left: Schematic of superficial cerebral vascular anatomy: A, superior sagittal sinus; B, lateral sinus; C, inferior cerebral vein. Right: Image of a mouse brain acquired *ex vivo* with a system based on Fabry-Perot interferometry.[68] (c) Whole-body image of a mouse acquired *in vivo*, where a 10-mm thick section of the abdomen is shown.[71]

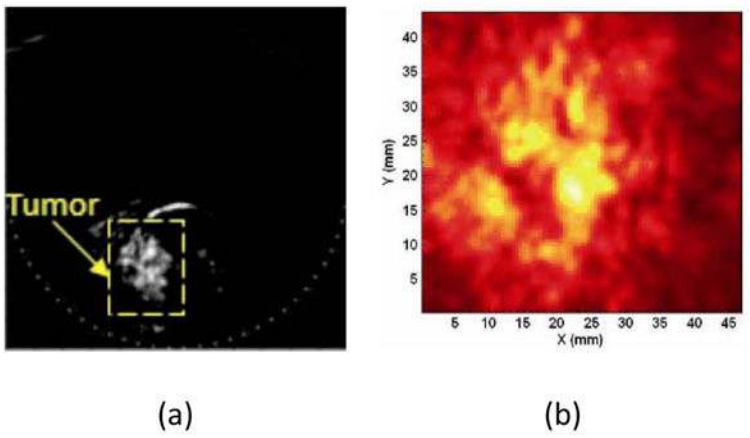

Figure 3. ***In vivo*** **photoacoustic computed tomography of the human breast acquired at 1064-nm laser wavelength**

(a) Image of a human breast containing a poorly differentiated infiltrating ductal carcinoma. The slice is 21 mm deep from the laser-illumination surface.[81] Field of view: 120 × 120 mm. (b) Image of a breast containing an invasive ductal carcinoma. The slice is 13.5 mm deep from the laser-illumination surface.82